Materials Horizons

ROYAL SOCIETY OF CHEMISTRY

COMMUNICATION

View Article Online
View Journal | View Issue

Cite this: *Mater. Horiz.*, 2024, **11**, 2010

Received 8th November 2023,
Accepted 29th January 2024

DOI: 10.1039/d3mh01884a

rsc.li/materials-horizons

Kirigami-enabled stretchable laser-induced graphene heaters for wearable thermotherapy†

Junyu Chen,‡[ab] Yichao Shi,§[a] Binbin Ying,¶[ac] Yajie Hu,[b] Yan Gao,[b] Sida Luo*[b] and Xinyu Liu*[ad]

Flexible and stretchable heaters are increasingly recognized for their great potential in wearable thermotherapy to treat muscle spasms, joint injuries and arthritis. However, issues like lengthy processing, high fabrication cost, and toxic chemical involvement are obstacles on the way to popularize stretchable heaters for medical use. Herein, using a single-step customizable laser fabrication method, we put forward the design of cost-effective wearable laser-induced graphene (LIG) heaters with kirigami patterns, which offer multimodal stretchability and conformal fit to the skin around the human body. First, we develop the manufacturing process of the LIG heaters with three different kirigami patterns enabling reliable stretchability by out-of-plane buckling. Then, by adjusting the laser parameters, we confirm that the LIG produced by medium laser power could maintain a balance between mechanical strength and electrical conductivity. By optimizing cutting-spacing ratios through experimental measurements of stress, resistance and temperature profiles, as well as finite element analysis (FEA), we determine that a larger cutting-spacing ratio within the machining precision will lead to better mechanical, electrical and heating performance. The optimized stretchable heater in this paper could bear significant unidirectional strain over 100% or multidirectional strain over 20% without major loss in conductivity and heating performance. On-body tests and fatigue tests also proved great robustness in practical scenarios. With the advantage of safe usage, simple and customizable fabrication, easy bonding with skin, and multidirectional stretchability, the on-skin heaters are promising to substitute the traditional heating packs/wraps for thermotherapy.

New concepts

This work demonstrates the new design and fabrication method of stretchable electrothermal heaters, which involve laser-induced graphene (LIG) to serve as resistive heaters and laser-cut kirigami to enable device stretchability. Based on a single-step laser engraving and cutting process, the LIG heaters and the kirigami structures are fabricated with customizable patterns to ensure heating uniformity, device stretchability, and wearing conformability for efficient on-skin thermotherapy. Different from existing wearable heater designs suffering from a complex and prolonged fabrication process, dispersion nonuniformity of conductive materials, and toxic chemical involvement, the conductive pathways and kirigami structures of the LIG heater can be readily adjusted based on the body location and curvature, and only a common CO_2 laser cutter is needed for device fabrication. We demonstrate the superior heating performance of the heater under multimodal loading as well as its practical application on the human body. This study highlights a new route to the development of low-cost, customizable, and mass-producible stretchable heaters for wearable thermotherapy.

[a] *Department of Mechanical and Industrial Engineering, University of Toronto, 5 King's College Road, Toronto, Ontario, M5S 3G8, Canada. E-mail: xyliu@mie.utoronto.ca*
[b] *School of Mechanical Engineering & Automation, Beihang University, No. 37 Xueyuan Road, Beijing, 100191, China. E-mail: s.luo@buaa.edu.cn*
[c] *Department of Mechanical Engineering, McGill University, 817 Sherbrooke Street West, Montreal, QC H3A 0C3, Canada*
[d] *Institute of Biomedical Engineering, University of Toronto, 164 College Street, Toronto, ON M5S 3G9, Canada*

† Electronic supplementary information (ESI) available. See DOI: https://doi.org/10.1039/d3mh01884a

‡ Current address: Department of Mechanical and Process Engineering, ETH Zürich, 8092 Zürich, Switzerland.
§ Current address: Department of Mechanical Engineering and Applied Mechanics, University of Pennsylvania, Philadelphia 19104, USA.
¶ Current address: Department of Mechanical Engineering, Massachusetts Institute of Technology, 77 Massachusetts Avenue, Cambridge, Massachusetts 02139, USA.

Xinyu Liu

Congratulations on the 10th Anniversary of Materials Horizons! We published our first MH article in 2020, which won the Outstanding Article Award of the year. I have been a loyal reader of MH because of its unique flavor of emphasizing new concepts and insights that very often bring true inspirations to me and my students. I wish Materials Horizons every success on reaching its next milestone and look forward to submitting our future best work to MH soon.

Introduction

An increasing number of people are suffering from muscle spasms, joint injuries, and arthritis. The annual medical cost for osteoarthritis is as high as 185.5 billion US dollars in the United States[1] and 408–817 billion euros in Europe[2] per year. Conventionally, chemical/electrical heating packs and wraps are employed to provide thermotherapy for injury and pain relief, tissue flexibility improvement, blood flow enhancement, and tissue repair acceleration.[3,4] However, issues such as mechanical rigidity, relatively slow heating-up, and/or limited functional time (in hours) exist for current chemical heaters,[3,5] while conventional electrical heaters have problems such as heavy weight, bulky volume, and poor portability.[4,5] In order to address the aforementioned shortcomings, significant efforts have been made to develop new types of wearable heating devices that are stretchable, lightweight, reusable, and inexpensive for practical thermotherapy.

In the past decade, flexible/stretchable electrothermal heaters have become a highly promising thermotherapy technology because of their wearing comfortability and practicability.[6,7] For example, conductive nanomaterials (*e.g.*, silver nanowires,[5] silver fractal dendrites,[8,9] carbon nanotubes,[10] and graphene-based materials[7]) have been dispersed into or coated on stretchable materials [*e.g.*, Ecoflex,[10] polydimethylsiloxane (PDMS),[11–13] and silk fibroin composite membrane[14]] to develop wearable electrothermal heaters. In addition, different mechanical designs of heating conductors (*e.g.*, serpentine mesh,[5,15] Archimedean spiral,[16] and kirigami[17–19]) have also been implemented in wearable heaters to achieve sufficient stretchability. However, there are still certain technical problems that hinder the practical use of these wearable heaters. For example, some existing heaters lack skin adhesion capability,[5–19] and the nanomaterial-based ones usually suffer from nonuniformity of nanomaterial dispersion in the stretchable materials.[20] Many stretchable heater designs involve prolonged material preparation and device fabrication processes (hours and even days),[6,11,14,17,21] and require sophisticated fabrication facilities.[15,16] The use of high-purity metals or carbon nanomaterials also leads to high fabrication costs,[5,11,12,14,18] and certain chemical compositions of the existing stretchable heaters (*e.g.*, xylenes, hydroiodic acid, xenon difluoride, and so on) also make them less biocompatible.[12,14,15,17,21–23]

Alternatively, laser induced graphene (LIG) is a conductive material that can be produced on plastic substrates through laser irradiation, and has unique features such as high versatility of material selection,[24] low cost and rapid production,[25] good compatibility with roll-to-roll processing,[26] customizable design,[27] and high performance tunability.[28] Benefiting from all these merits, LIG has been widely applied for developing actuators,[29] sensors,[30] supercapacitors,[31] and so on. Recently, LIG has also been employed to fabricate high-performance flexible electrothermal heaters with excellent flexibility, customizable structure, uniform temperature distribution, and high mechanical and thermal robustness.[25,26] For example, Bobinger *et al.*[25] fabricated an LIG heater directly on a piece of flexible polyimide (PI) film. Chen *et al.*[26] studied the multimodally patternable performance of LIG heaters and applied them to *in situ* manufacturing of composites. However, because of the limited elongation at break and high modulus of the PI substrate, the LIG heater generally has poor stretchability. As a result, it is hard for a PI-based LIG heater to match both softness and stretchability (up to $\sim$50%) of human skin;[32] with such a LIG heater on skin, the body movement in arbitrary directions will be impeded. Although transferring LIG onto a PDMS substrate could enhance the capability of stretching and reduce the modulus of wearable LIG heaters,[13] the limited stretchability ($<$20%) and sacrificed heating uniformity (due to the fracture of conductive LIG pathways) of such a device still cannot meet the requirement of wearable thermotherapy. Hence, new LIG heater designs are still needed to achieve both good electrothermal performance and high device stretchability.

In this study, we propose a new design of stretchable LIG heaters with novel kirigami patterns. With a single-step laser manufacturing method, we simultaneously endow a PI substrate with both LIG-based conductive pathways and stretchable kirigami structures. The high device stretchability is achieved through three kirigami designs that are customized and optimized based on different on-skin wearing locations, providing a personalized thermotherapy solution for practical medical use. Stretchable and biocompatible elastomers, including Ecoflex silicone rubber and high-performance adhesive tape (VHB), are chosen for encapsulation and skin adhesion of the LIG heater. We demonstrate that the stretchable LIG heater can achieve rapid temperature escalation, capable of reaching over 40 °C within 1 min at a voltage supply of $<$36 V, which is safe for on-body wearing.[33] We perform both finite element simulation and experimental testing to optimize the kirigami design parameters to accomplish robust unidirectional stretchability of 100% and multidirectional stretchability of 20%, with no obvious sacrifice in both conductivity and heating performance of the LIG heater. The stretchable LIG heater is customizable-in-design, lightweight, low-cost, safe-to-operate, comfortable-to-wear, and provides multimodal stretchability. This novel wearable technology will lead to a practical solution for personalized wearable thermotherapy.

Results and discussion

Design and characterization of the LIG heaters

Fig. 1a illustrates the overall fabrication process of the unidirectionally and multidirectionally stretchable heaters. The wearable heater consists of a LIG heating layer, a silicone rubber cover layer and a VHB adhesive layer. Pre-designed using computer aided design software, the LIG conductor and kirigami patterns could be produced on a PI film through single-step laser cutting. Moreover, the customizable design and scalable roll-to-roll fabrication[26] of LIG will enable the mass production of wearable heaters to meet high-volume demands from different patients. Firstly, with a lower laser power, only the top surface

of the PI film was carbonized into conductive LIG, while the bottom portion of the PI film remained intact and thus served as the structural substrate. Afterwards, the PI film was cut through by laser with a higher power level to form kirigami patterns. The laser-patterned LIG heater was finally encapsulated with Ecoflex and VHB, which allows the heater to operate safely (with proper electrical insulation) and conformally adhere (through the adhesive VHB) to skin. The high stretchability and biocompatibility of the Ecoflex and VHB have been demonstrated in a wide range of applications, such as soft robotics,[34] epidermal electronic interfaces,[35] skin-mounted power management systems,[36] triboelectric nanogenerator,[37] and so on. The two encapsulation layers also endow the electrothermal heater with homogeneous temperatures.

We designed two kirigami patterns to achieve the unidirectional and multidirectional stretchability of the LIG heater (see design details in the section on Design and Optimization of Kirigami Patterns). Fig. 1b and c show photographs of two types of heaters being stretched with different strain levels. One can see that the cutting lines of kirigami patterns opened up when the heater was under large deformation. No macroscopic fracture was observed on the unidirectional heater under strains of $\leq$100% and on the multidirectional heater under strains of $\leq$15% along the x, y, or both directions. In order to further investigate the heater performance under biaxial tension, the multidirectional heater was attached to an inflatable balloon. The multidirectional heater maintained a uniform temperature distribution when the balloon was inflated from 17 cm to 25 cm in length (Fig. 1d).

Prior to testing the mechanical, electrical, and electrothermal performance of the LIG heaters, we first characterized the component materials of the LIG. Fig. 1e shows the SEM image of the LIG with randomly oriented and entangled fibers, which is a typical morphology of the LIG.[28] Fig. S1 (ESI†) further compares the microstructures of a LIG heater with unidirectional kirigami patterns (at three magnification levels) before and after 100 times of cyclic stretching at 100% strain. No obvious morphological and structural difference was observed before and after the cyclic stretching, confirming that the kirigami/LIG patterns have high mechanical robustness under large cyclic strains. The Raman spectrum shown in Fig. 1f reveals distinct D, G and 2D peaks (at 1339 cm^{-1}, 1567 cm^{-1} and 2671 cm^{-1}), indicating few-layer graphene in the LIG.[38] The XRD spectrum (Fig. 1f) reveals peaks at 25.72° and 42.64° representing (002) and (100) respectively, which further verified the multilayered in-plane structure of the LIG with an interlayer spacing of 0.34 nm.[39] An excessively high laser power level may result in cutting through the PI film, whereas an insufficiently low laser power level fails to effectively transform PI into LIG. We experimentally determined that the appropriate laser power range for fabricating LIG on a PI film of 50 μm thickness is 8.25–13.25 W with a laser cutting speed of 889 mm s^{-1}. As shown in Fig. S2, laser (ESI†) irradiation within this power range yielded LIG with proper Raman spectra. With the laser power increased from 8.25 W to 13.25 W, we found that the sheet resistance of LIG decreased from $\sim$204 Ω sq^{-1} to $\sim$139 Ω sq^{-1} (Fig. 1g) because of the increased thickness of the formed LIG.[28] However, in the meantime the tensile strength of the kirigami structure decreased accordingly (Fig. 1g) because of the decreased thickness of the remaining PI substrate. In the following experiments, we chose a 10.75 W laser to fabricate LIG heaters to reach a good balance of the mechanical and electrical properties of the heater.

Design and optimization of kirigami patterns

Although the LIG heater on a continuous PI film is mechanically robust, tensile tests revealed its drawback of high Young's modulus ($\sim$470 MPa; data shown in Fig. S3, ESI†), which is about three orders of magnitude higher than skin.[40] Its electrical resistance variation is $\sim$100% when the elongation is only $\sim$10% (Fig. S3, ESI†). Therefore, kirigami structures, which have been widely utilized for soft robots,[41] strain sensors,[42] metasurfaces,[43] and stretchable power packages,[44] were introduced to improve the stretchability of the LIG heater. To accommodate varying stretchability requirements across different parts of the human body, we meticulously designed and tested two kirigami patterns. The first pattern has interlaced line segments and is unidirectionally stretchable (Fig. 2a). The geometric parameters to define this pattern are a, d and l (Fig. 2a), representing the hinge length, hinge spacing, and cut length. The second pattern consists of repeated three-point star cutting lines (Fig. 2b). The critical parameters of this pattern are b and s, representing the arm length and horizontal pitch of the three-point star pattern.

To streamline the parameter tuning, we standardized certain dimensions, setting a = 2 mm, l = 6 mm, and s = 5 mm. We then focused on adjusting two key dimensionless variables $r_1 = l{:}\ d$ and $r_2 = b{:}\ s$, which are defined as the cutting-spacing ratios. Finite element analysis (FEA) shows that both kirigami structures have good stretchability, which are realized through the combination of in-plane and out-of-plane deformations (Fig. 2c–e). The FEA data of average stress *vs.* strain (Fig. 2f–h) show a typical three-stage curve of the kirigami structures: in-plane stretching, out-of-plane bending, and out-of-plane stretching.[42] The secant modulus at 100% elongation is only $\sim$0.05 MPa when r_1 = 12, which is 4 magnitudes smaller than the modulus of LIG without kirigami patterns (Fig. S3, ESI†). The relationship of the relative electrical resistance change *vs.* strain reveals a similar trend as the corresponding stress–strain curve (Fig. 2f–h). For both mechanical and electrical properties, the unidirectional pattern with larger r_1 has better stretchability among all of the designs (r_1 = 3, 6 and 12).

With the optimal parameter we have chosen, there is only $\sim$10.8% rise in electrical resistance when ε_{xx} = 1, while the resistance ascent of the uncut LIG film exceeds 95% under 0.1 strain (Fig. S3, ESI†). The degradation of conductivity was probably caused by microscale cracks that partly interrupt the conductive pathway of the LIG and electrodes.[45] Subsequently, we studied mechanical and electrical properties in both x and y directions for the multidirectional heater (Fig. 2g and h). Since the hinge length of multidirectional heater is smaller, stress concentrations at the hinges make this kirigami structure more likely to fracture under large strain. Thus, the maximum

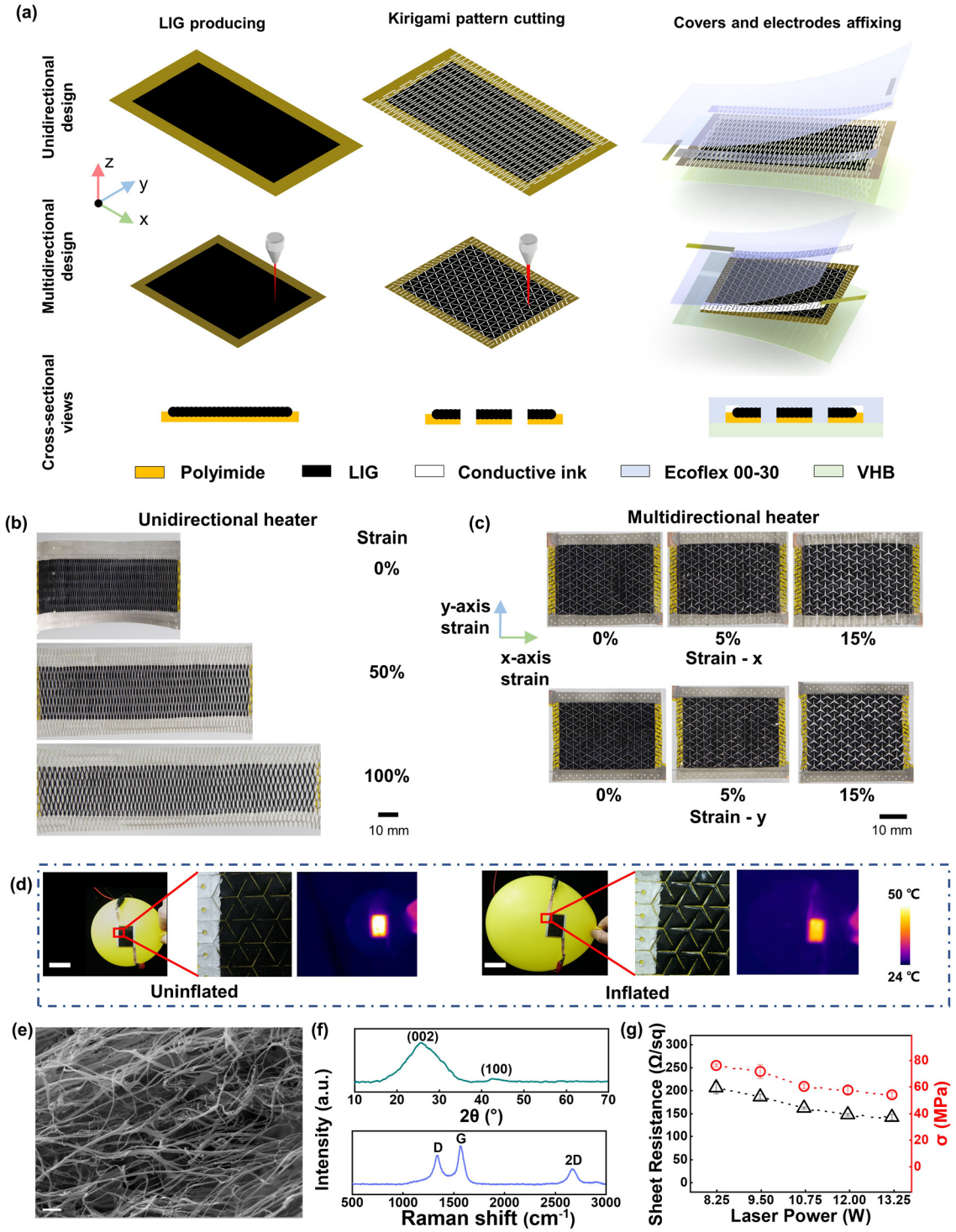

Fig. 1 Heater design and characterization. (a) Schematic diagram of heater design and fabrication. (b) Unidirectional heater stretched from 0 to 100% strain (scale bar: 10 mm). (c) Multidirectional heater stretched in the *x* and *y* directions (scale bar: 10 mm). (d) Multidirectional heater stretched in both *x* and *y* directions on an inflated balloon (scale bar: 50 mm). (e) SEM image of LIG with kirigami cutting patterns (scale bar: 1 μm). (f) XRD (bottom) and Raman (top) spectra of the LIG. (g) Stress/resistance variation – strain relationship of the LIG.

strain of multidirectional heater is smaller than its unidirectional counterpart. Through further tensile tests, it is found that larger values of cutting-spacing ratios in ranges of 0.45, 0.4, and 0.35 can offer better stretchability, *i.e.*, smaller relative resistance variation/stress under the same strain. However, the scope of cutting-spacing ratios is also restricted by fabrication and practical use. Parameter d cannot be too small and b cannot be too large because the hinge and spacing between neighboring cutting

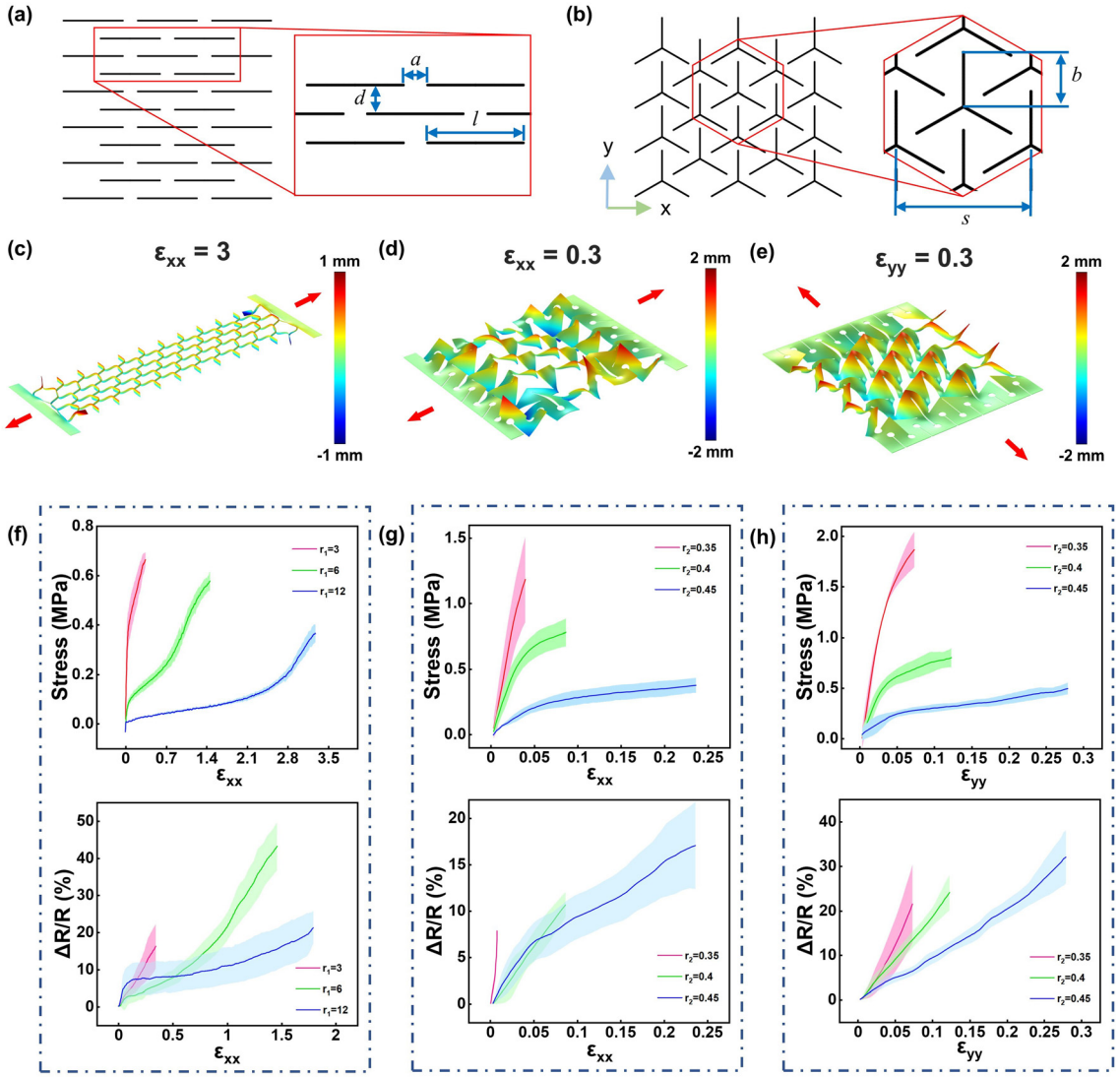

Fig. 2 Kirigami design and optimization. (a) Unidirectional kirigami pattern. (b) Multidirectional kirigami pattern. (c)–(e) *z*-direction displacement of LIG with kirigami cutting in FEA. (c) Unidirectional kirigami. (d) Multidirectional kirigami stretched in the *x* direction. (e) Multidirectional kirigami stretched in the *y* direction. (f)–(h) Experimental measurement of average stress and resistance variation *versus* strain for LIG with kirigami cutting. The shade around the curves represents the standard deviation. (f) Unidirectional kirigami. (g) Multidirectional kirigami stretched in the *x* direction. (h) Multidirectional kirigami stretched in the *y* direction.

lines are prone to break due to the machining error and local stress concentration. Thanks to the kirigami structure, the average stress and relative resistance variation are orders of magnitude smaller compared to the whole piece of LIG. With the huge improvement in stretchability, the LIG heaters were able to be conformally attached on the skin.

Mechanical and electrical characterization

Fig. 3a–c illustrate the exploded views of the FEA results for the unidirectional and multidirectional LIG heaters with the top Ecoflex layer and the bottom VHB layer (see details in the Experimental section). Due to the modulus difference of the three layers, the maximum stress on the LIG layer is 2–3 orders of magnitude higher than that on the two encapsulation layers. The stress concentration of the LIG layer mainly occurred at the endpoints of laser cutting lines. After encapsulating the unidirectional LIG layer with the two elastomer layers, the modulus of the trilayer heater becomes ~5 times higher than that of the bare LIG layer (Fig. 3d); this is due to the constraint of the two elastomer layers on the out-of-plane deformation of the kirigami structure. The limited out-of-plane deformation of the kirigami structure in the trilayer structure also facilitates the conformal adhesion of the LIG heater on skin during stretching. The trilayer LIG heater also revealed a larger relative resistance change (Fig. 3d). Note the secant modulus of the trilayer LIG heater (0.233 MPa calculated from Fig. 3d) still matches the modulus of human skin (0.42–0.85 MPa),[40] which means that the heater will not obviously hinder the free movement of the human body.

Tensile tests were then carried out to compare the stretchability of unidirectional heaters with different cutting–spacing

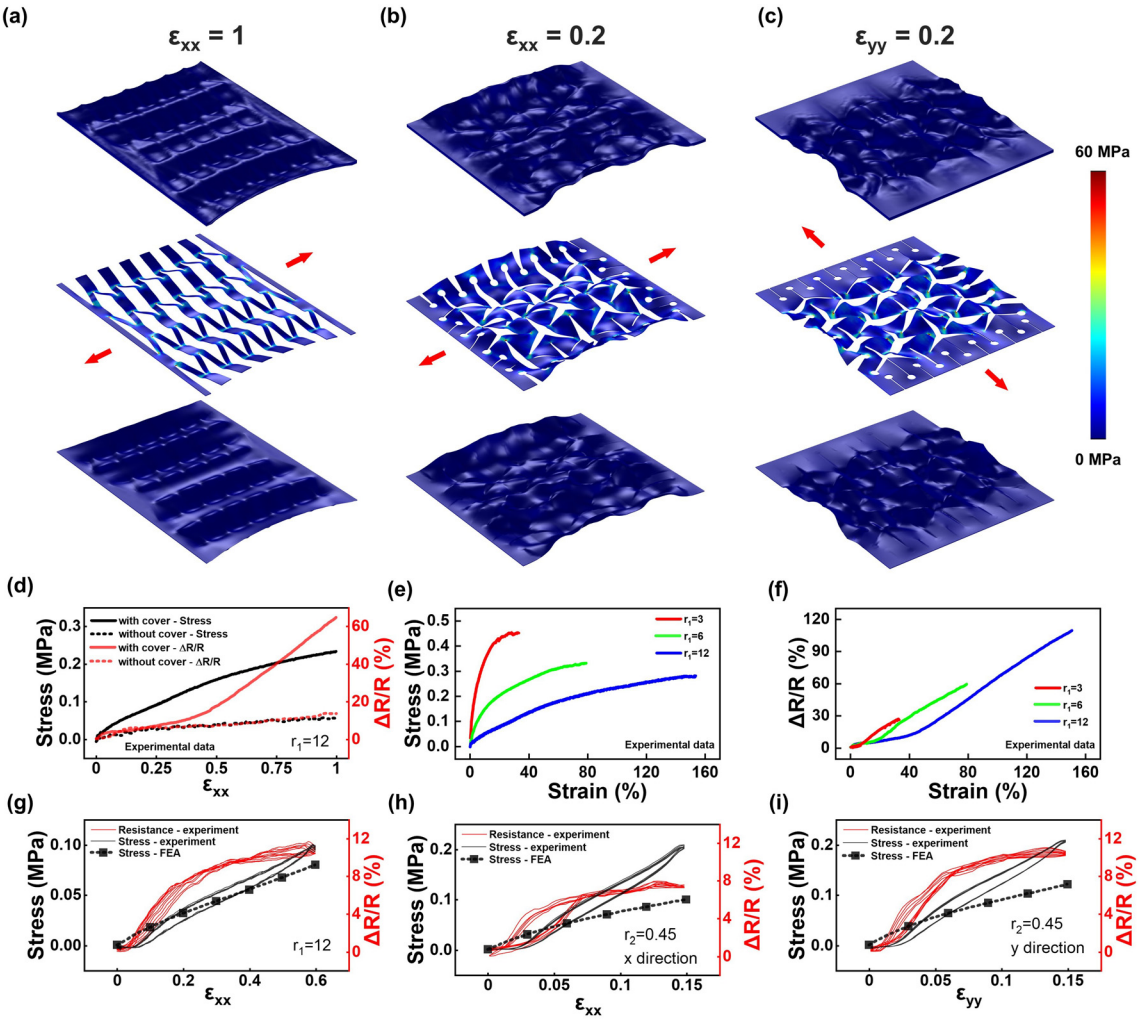

Fig. 3 Mechanical and electrical characteristics of the heater. (a)–(c) Exploded view of heaters in FEA. The three layers are Ecoflex, LIG and VHB from top to bottom. (a) Unidirectional kirigami. (b) Multidirectional kirigami stretched in the *x* direction. (c) Multidirectional kirigami stretched in the *y* direction. (d) Experimental comparison in mechanical and electrical properties between the kirigami structure with and without the covers (unidirectional heater, r_1 = 12) (e) Experimental comparison of stretchability characterized by stress–strain relationship. (f) Experimental comparison of stretchability characterized by resistance variation-strain relationship. (g)–(i) Stress and resistance variation as functions of strain. (g) Unidirectional heater. (h) Multidirectional heater deformed in the *x* direction. (i) Multidirectional heater deformed in the *y* direction.

ratios (r_1). Fig. 3e and f show the measured stress–strain curves and resistance variation–strain curves of the unidirectional heater (with encapsulation layers) with r_1 = 3, 6, and 12. One can see that at the same stress level or resistance variation level, the heater with a higher r_1 value always yields a higher elongation. Thus, in final designs of the unidirectional and multidirectional heaters, the cutting–spacing ratios are set to be r_1 = 12 and r_2 = 0.45. With a maximum strain of ε_{xx} = 0.6, a unidirectional heater was pre-stretched for 10 cycles, and values of the stress and the relative resistance change of the heater were then experimentally recorded as functions of strain for another five cycles (Fig. 3g). The secant Young's modulus of the unidirectional heater was calculated to be 0.169 MPa, which is comparable to the FEA result (0.133 MPa). The relative resistance change was within 12% with an elongation of 60%, and this small resistance change will not significantly affect the electrothermal performance of the heater (data shown in the section on Electrothermal characterization). For the multidirectional heater, 10 pre-stretching cycles at 15% strain were applied along the *x* or *y* direction, and the stress and relative resistance change data were then recorded for another five cycles along the same direction. based on the experimental stress–strain curves in Fig. 3h and i, the secant Young's moduli of the multidirectional heater were calculated to be 1.43 MPa along the *x* direction and 1.43 MPa along the *y* direction, which are higher than that of the human skin (0.42–0.85 MPa). However, since the heater only has a thickness of 0.35 mm, the total force needed to stretch the multidirectional heater to 15% strain in the *x* or *y* direction is only up to 3 N. The maximum relative resistance changes of the multidirectional heater are within 12% at the 15% strain. To sum up, both types of LIG heaters with the two encapsulation layers have low Young's moduli approximately matching the skin modulus and only yield relatively low resistance change (<12%) upon

stretching. In addition, a T-peeling test is carried out to verify that the LIG heaters have good adhesion to skin (Fig. S4, ESI†). These results indicate that the heaters have robust mechanical and electrical properties suitable for use as wearable heaters for thermotherapy.

Electrothermal characterization

Apart from good mechanical and electrical properties under stretching, the heaters also exhibit appropriate electrothermal performance for thermotherapy. Fig. 4a illustrates the transient profile of temperature *vs.* time of the unidirectional heater under a DC voltage for 120 s. Considering it as a pure resistor, the electrical power of the heater was fully converted into thermal energy. As the DC voltage increases, the total input electrical power ($P = V^2/R$) becomes higher, which leads to a higher steady state temperature (T_s) of the heater. The heater achieved a temperature rise of 32.2 °C (average of the temperature curve from 60 s to 120 s in Fig. 4a) at 10 V voltage, which is sufficient for thermotherapy.[46] The required voltage (10 V) is within the safe range of operation for wearable devices on the human body.[33]

Another important electrothermal parameter is the time required for the heater to reach its thermal equilibrium stage. The total temperature rise of the heater is $\Delta T = T_s - T_0$, where T_0 is the ambient temperature. The temperature rising time t_r is counted as the total time from the power-on time point to the point that the heater temperature exceeds 90% of ΔT.[26] Then, we define the temperature ramp rate r = 90% $\Delta T/t_r$. Based on data in Fig. 4a, t_r is always within 51 s in the voltage range of $\leq$10 V. In contrast, t_r of the traditional chemical heating pack is approximately 760 s (Fig. S5, ESI†). The insets of Fig. 4a show the measured ΔT and r values as functions of the input DC voltage. One can see that both ΔT and r increase with the input voltage, and at 10 V it only takes 43 s for the unidirectional heater to reach a temperature rise of 29.6 °C (r = 0.69 °C s^{-1}). The high ramp rate and short temperature rising time of the stretchable heater ensure that a user will have their treatment site warmed up rapidly after the heater power turns on. Fig. S6

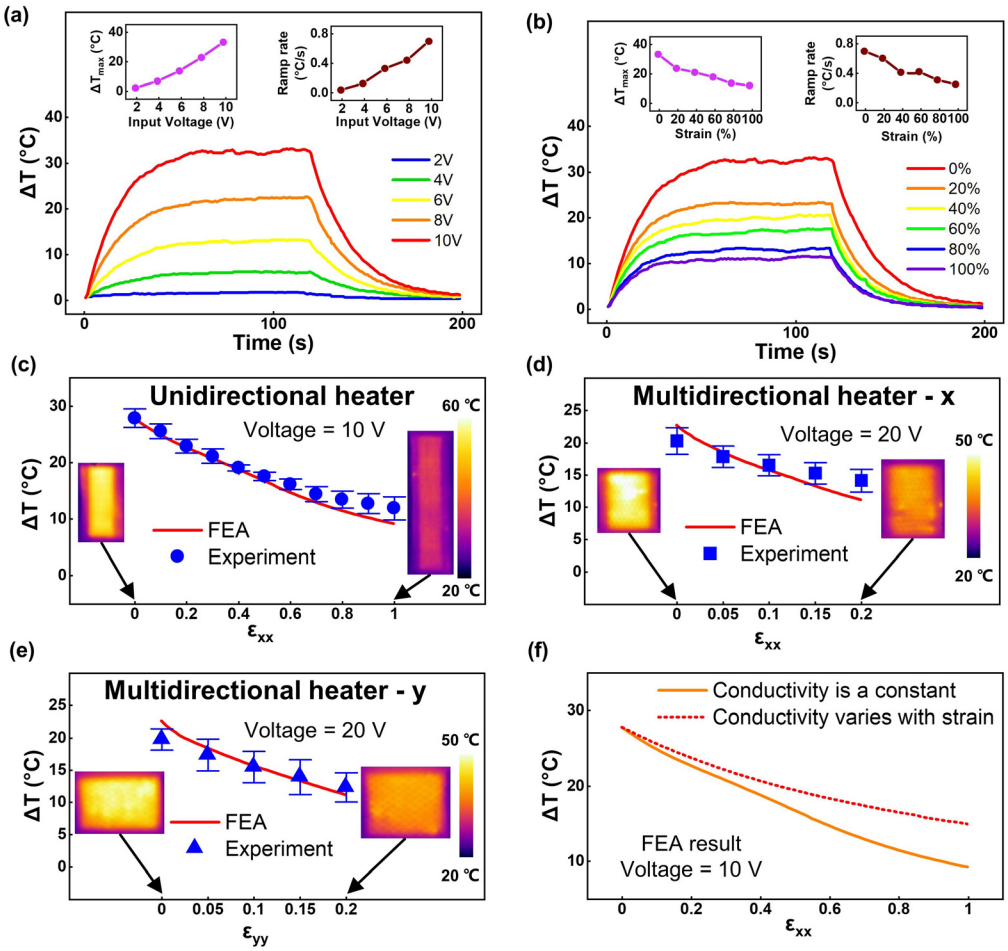

Fig. 4 Electrothermal characterization. (a) Transient temperature response under different input voltages (unidirectional heater, r_1 = 12, strain = 0. Insets: maximum ΔT and ramp rate at different input voltage). (b) Transient temperature response under different strain (unidirectional heater, r_1 = 12, input voltage = 10 V. Insets: maximum ΔT and ramp rate at different strain). (c)–(e) Steady state average temperature as a function of strain (c) Unidirectional heater with r_1 = 12 (Insets: heat maps of the heater at 0 and 100% strain). (d) Multidirectional heater with r_2 = 0.45 (Insets: heat maps of the heater at 0 and 20% strain in the x direction). (e) Multidirectional heater with r_2 = 0.45 (Insets: heat maps of the heater at 0 and 20% strain in the y direction). (f) Variation of average temperature as a function of strain in FEA.

(ESI†) shows similar results for the multidirectional heater. We also recorded the heating and cooling profiles of the unidirectional and multidirectional heaters at different tensile strain levels (Fig. 4b and d). T_s and r decrease with the tensile strain, which is due to the strain-induced increase of the heater resistance ($P = V^2/R$). However, t_r can still be maintained at a relatively low level within 60 s, which means that large deformation has little effect on the warm-up time.

To verify that the heater could withstand large deformation and maintain heating performance, infrared (IR) imaging was also conducted on the LIG heaters during tensile testing. Fig. 4c–e show the total temperature rise (ΔT) of the unidirectional (Fig. 4c) and multidirectional (Fig. 4d and e) heaters as a functional of strain, from both FEA and IR measurements. Fig. 4c includes the IR thermograms of the unidirectional heater with and without 100% tensile strain, and both images show uniform temperature distributions across the main area of the heater. It is worth mentioning that the two encapsulation elastomer layers serve as thermal homogenizers by conducting heat from the LIG patterns to the rest of the PI film areas, so that the entire heater reaches uniform temperature distributions with and without stretching. Moreover, compared with a previously reported kirigami-based heater with the cover layer cut through,[18] a continuous cover layer provides a larger effective heating area contacting the skin for more efficient thermotherapy. With a fixed input voltage of 10 V, the total temperature rise (ΔT) of the unidirectional heater decreases from 27.9 °C to 11.9 °C when the heater is stretched for 100%. For a realistic strain range ($\leq$50%) of human skin during body movement, ΔT drops to 17.57 °C. If a constant heater temperature is desired during on-body wearing, LIG-based temperature sensors[47] can be co-fabricated on the heater for closed-loop temperature control. Fig. 4d and e illustrate the maximum temperature rise of the multidirectional heater with a strain of 0–20% along the x and y directions, respectively (input voltage: 20 V). ΔT was found to be 14.13 °C and 12.33 °C at the maximum strain of 20% along the x and y directions, respectively.

For the purpose of finding out the main reason, we assumed that the conductivity was a constant in the FEA model. In this case, the main factor that could result in a temperature drop was the enlarged heat dissipation area. Compared with the normal case, the drop in temperature only reduced by ~30% (Fig. 4f). The major factor that affects the heating temperature, enlarged heat dissipation area, is inevitable when the heater is under stretching. A possible solution in practical use is introducing feedback control in the power source and providing higher input power when the heater is elongated, which will compensate the extra heat dissipation. In summary, the heater can swiftly warm up and preserve a uniform temperature profile under large strain.

On-body testing

Finally, on-body testing of the LIG heaters was carried out on different parts of the human body. Fig. 5a shows optical and IR images of the heaters with different stretching modes. For body joints such as the wrist, elbow, and knee, the major stretching direction of the skin is along the longitudinal direction of the joint. Thus, the unidirectional heater is suitable for attachment on body joints. Taking the elbow as an example (the first row of Fig. 5a), the heater is unstretched when the arm is straight; when the elbow bends about 90°, the heater can conformally extend with the elbow skin and warm up the skin uniformly to maximum 39 °C in 2 min (input voltage: 10 V). Multidirectional strains usually occur on the back area when adducting the shoulders in and in the meantime stooping down. As shown in Fig. 5a (2nd row), the temperature of a multidirectional heater attached to the upper-right area of the human back was measured to be ~41 °C when the heater is unstretched, and dropped to ~40 °C when the heater was stretched. The multidirectional heater always maintained good temperature uniformity, suggesting good electrothermal performance during body movements.

Thanks to the flexible kirigami design and single-step laser cutting/scribing technique, heaters with tailored kirigami patterns could be designed and manufactured to satisfy personalized demands. For example, to accommodate the out of plane motion of the shoulder tip, a heater with concentric annulus kirigami patterns has been designed and fabricated. Fig. S7 (ESI†) illustrates the layout, the electrode arrangement, and the deformation mode of the kirigami pattern. When lifting the arm horizontally, the skin on the shoulder is flat. When laying down the arm, the shoulder turns into a spherical shape. The temperature profile of the heater (the third row of Fig. 5a) is highly uniform no matter the arm is raised or lowered.

We also performed long-term on-body testing of the unidirectional heater for warming up the wrist. The on-wrist heater was initially warmed up to 38.5 °C under 10 V. Then, the wrist was repeatedly bent to its limit for 100 cycles, and the heater temperature was constantly monitored. As shown in Fig. 5b, the heater temperature only fluctuated within 0.81 °C, demonstrating the mechanical/electrical robustness and the stable electrothermal properties of the heater. The good electrothermal stability of the heater is further verified by 100 power on/off cycles (Fig. S8, ESI†). Cyclic tensile testing of the unidirectional heater was also conducted for 1000 cycles with a maximum strain of 60% (Fig. 5c). The maximum relative resistance change during one-time stretching was ~7.5%, and the baseline of the heater resistance shifted by ~4.8% after 1000 stretching cycles. The stress at 60% strain remained stable at ~0.1 MPa with little stress relaxation at the first several cycles. The resistance baseline shift could be attributed to the nanostructure change of the LIG after a large number of related stretching.[45,48]

Conclusions

The single-step laser production process, which synergistically integrates the kirigami structure and LIG, opens up a new route to stretchable electrothermal heaters with good safety and affordability, stable heating performance, fast and

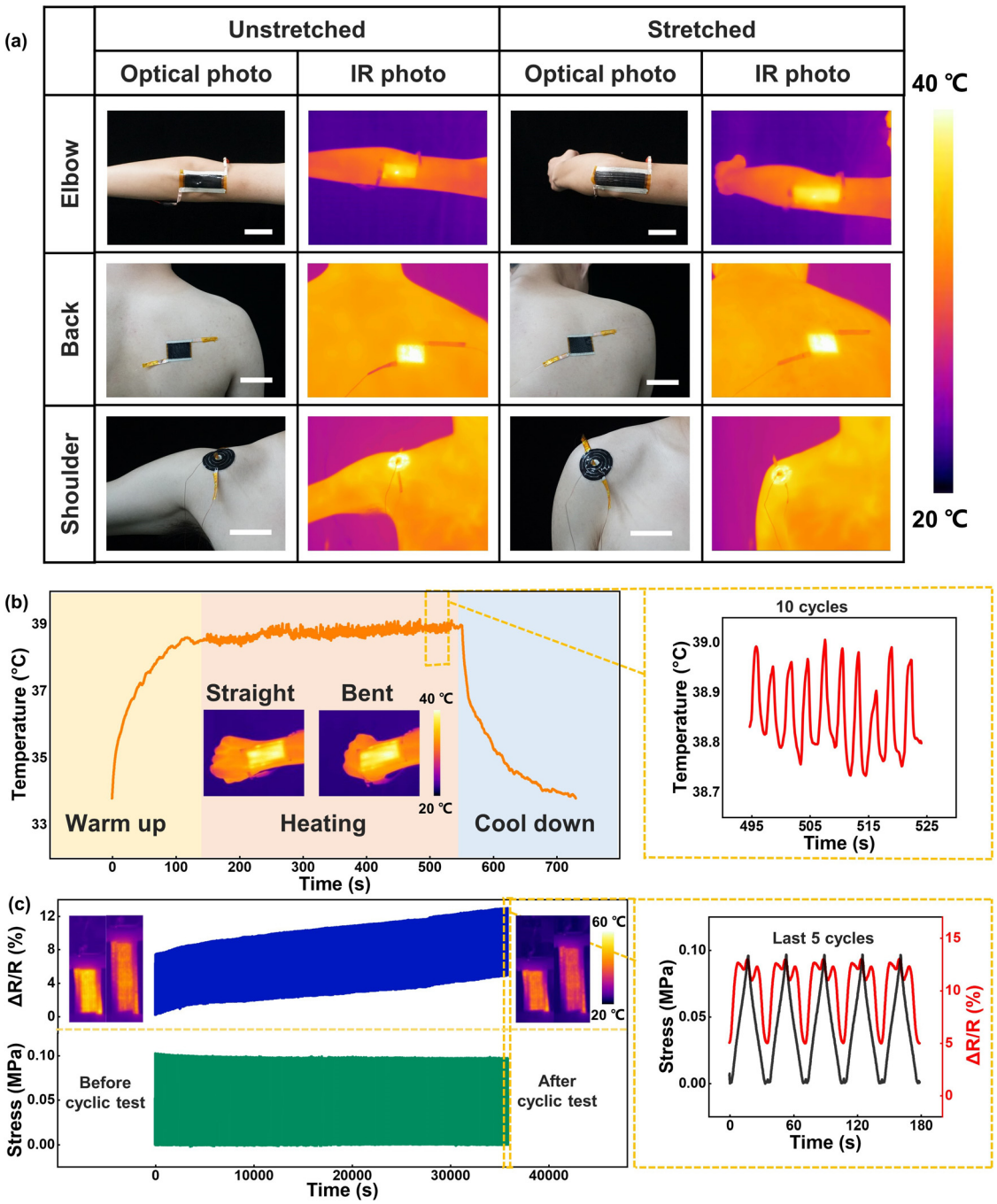

Fig. 5 Practical demonstration. (a) *In vivo* tests of three types of heaters (scale bar: 50 mm). (b) Long time on body test (Insets: thermograms of the heater on the wrist). (c) Cyclic deformation between 0 and 60% strain for 1000 times (Insets: infrared photo of the heater at 0 and 60% strain before and after 1000 deformation cycles).

straightforward fabrication. The application of VHB and Ecoflex as covering materials enables the heater to adhere conformally to symptomatic areas and to warm up homogeneously while offering additional protection to both the heater and the human skin. After meticulous design and optimization, both unidirectional and multidirectional heaters can retain their conductivity and advanced temperature uniformity within the range of skin deformation. In addition, the lightweight nature of these heaters and fast transient temperature response (<1 minutes) make them significantly surpass the traditional heating packs/wraps in terms of efficiency and convenience. On-body tests have further validated the heater's versatility and effectiveness in thermotherapy across various body positions and under different forms of deformation. 1000 stretching and relaxing cycles also testified the good durability of the heater. Demonstrating the concept of customized *in situ*

manufacturing for instant medical use, this heater could become a powerful tool in medical treatment and daily life, offering a versatile and powerful tool for future healthcare solution.

Experimental section

Fabrication of the LIG heater

A commercial CO_2 laser cutter (10.6 μm wavelength, ~100 μm focal beam, DLS 2.3, Universal Laser Systems, Inc.) was first applied to scan on surface of the PI film (Kapton, 50 μm) to produce LIG. With a laser power ranging from 8.25 to 13.25 W, a line space of 50 μm, an image density of 500 pixels per inch (PPI) and a scan rate of 889 mm s^{-1}, only the surface layer of PI film was transformed into LIG. Afterwards, the PI film was cut through using a 7.5 W laser with a scan rate of 254 mm s^{-1} to present kirigami patterns. Stretchable electrodes are made by conductive silver ink (Jingling Co.) covering the juncture of PI and LIG. As a result, a serpentine conductive pathway formed on the opposite edges of the kirigami structure. Copper tapes were attached to the ends of stretchable electrodes for connecting to the power source. Then the heaters were placed on the 100 °C heating stage for 30 minutes to solidify the silver ink. A piece of VHB (F9460PC, 3 M Co., 50 μm in thickness) was adhered to the PI side of the heater. After defoaming the uncured silicone rubber, the elastomer (Ecoflex 00-30, Smooth-on inc.) was spin coated at 1000 rpm for 30 s on the LIG side to yield a ~200 μm cover layer. Ecoflex can infiltrate into the laser cutting gaps and bond with VHB after curing at 100 °C for 20 minutes.

Characterization of LIG

To identify the graphitic microstructures of laser processing, a ZEISS SUPRA55 was adopted to take scanning electron microscopy (SEM) images at 15 kV with platinum sputtering. A Horiba HR800 Raman microscope using a 5 mW 532 nm excitation laser was employed to obtain Raman spectra. And X-ray diffraction (XRD) was conducted on a Rigaku Ultima IV instrument with Cu Kα radiation $\lambda = 1.54^{\circ}$.

Evaluation of mechanical and electrothermal properties

Tensile tests were carried out on an E44.104 tensile testing machine (MTS Systems Corp.). Dog bone samples of Ecoflex and VHB were prepared and their stress–strain curves were used for the hyperelastic models. The heaters were subjected to tensile test with a displacement rate at 200% gauge length per min. The gauge lengths were 70 mm, 30 mm and 25 mm for unidirectional heater and multidirectional heater in x and y directions. Meanwhile, the heaters were powered by Keithley 2450 Sourcemeter and the data of electrical resistance variation was recorded using the sourcemeter connected to KickStart software. Thermograms were taken by an infrared camera (FLIR T420) and analyzed using FLIR tools software.

Finite element analyses (FEA)

Simulation software COMSOL Multiphysics was utilized to conduct the FEA on stretchable heaters, which included the mechanical and electrothermal behaviors. Considering the incompressible hyperelastic characteristics of the materials, Yeoh[49] hyperelastic models (Fig. S9, ESI†) were employed for Ecoflex and VHB. The parameters for the Yeoh model were acquired by fitting the stress–strain curve from the tensile test. In order to simplify the model, LIG with a PI substrate was considered as a homogeneous material, the square resistance of which was the same as LIG. Triangular meshes swapping in the thickness direction were applied in all FEA. And refined meshes at endpoints of the cutting lines could improve the accuracy in the physical fields with a large stress gradient. We enforced fixed boundaries on one end. To guarantee the out of plane buckling, on the opposite end, we set a displacement in the direction perpendicular to the heater that the perturbation was small enough (<1% length of the heater) to have little effect on the stress–strain relationship. The FEA was first applied to optimize the design of the kirigami structure without the covers. Then we studied the mechanical and electrothermal performance of the whole heaters. The surface meshes on the interfaces between different layers of the heater share the same nodes. As a result, the simplified interfaces between different materials won't have any relative motion. In order to reduce the amount of computation, we only select a fraction of the physical model in the FEA.

Conflicts of interest

There are no conflicts to declare.

Acknowledgements

This research was supported by the Natural Sciences and Engineering Research Council of Canada (RGPIN-2017-06374, RGPAS-2017-507980, RGPIN-2022-05039, and RTI-2021-00769) and the Canada Foundation for Innovation (JELF-38428). The authors also acknowledge financial support from the University of Toronto through the Percy Edward Hart Professorship (to X. Liu), the China Scholarship Council grant no. 201906020290 (to J. Chen). S. Luo acknowledges the financial support from the National Natural Science Foundation of China (62371025 & T2121003) and the Beijing Natural Science Foundation (3202017).

References

1 H. Kotlarz, C. L. Gunnarsson, H. Fang and J. A. Rizzo, *Arthritis Rheum.*, 2009, **60**, 3546–3553.
2 J. H. Salmon, A. C. Rat, J. Sellam, M. Michel, J. P. Eschard, F. Guillemin, D. Jolly and B. Fautrel, *Osteoarthr. Cartil.*, 2016, **24**, 1500–1508.
3 J. S. Petrofsky, M. Laymon and H. Lee, *Med. Sci. Monit.*, 2013, **19**, 661–667.
4 S. Michlovitz, L. Hun, G. N. Erasala, D. A. Hengehold and K. W. Weingand, *Arch. Phys. Med. Rehabil.*, 2004, **85**, 1409–1416.

5 C. Suji, P. Jinkyung, H. Wonji, K. Jangwon, K. Jaemin, L. Young Bum, S. Changyeong, H. Hye Jin, K. J. Hoon and H. J. A. N. Taeghwan, *ACS Nano*, 2015, **9**, 6626–6633.
6 D. I. Moon, G. Plečkaitytė, T. Choi, M. L. Seol, B. Kim, D. Lee, J. W. Han and M. Meyyappan, *Adv. Healthcare Mater.*, 2020, **9**, 1901575.
7 A. Hazarika, B. K. Deka, D. Kim, H. E. Jeong, Y. B. Park and H. W. Park, *Nano Lett.*, 2018, **18**, 6731–6739.
8 P. Zeng, B. Tian, Q. Tian, W. Yao, M. Li, H. Wang, Y. Feng, L. Liu and W. Wu, *Adv. Mater. Technol.*, 2019, **4**, 1800453.
9 B. Tian, Q. Liu, C. Luo, Y. Feng and W. Wu, *Adv. Electron. Mater.*, 2020, **6**, 1900922.
10 Y. Lee, V. T. Le, J.-G. Kim, H. Kang, E. S. Kim, S.-E. Ahn and D. Suh, *Adv. Funct. Mater.*, 2018, **28**, 1706007.
11 H. Kim, M. Seo, J. W. Kim, D. K. Kwon, S. E. Choi, J. W. Kim and J. M. Myoung, *Adv. Funct. Mater.*, 2019, **29**, 1901061.
12 S. Hong, H. Lee, J. Lee, J. Kwon, S. Han, Y. D. Suh, H. Cho, J. Shin, J. Yeo and S. H. Ko, *Adv. Mater.*, 2015, **27**, 4744–4751.
13 D. X. Luong, K. Yang, J. Yoon, S. P. Singh, T. Wang, C. J. Arnusch and J. M. Tour, *ACS Nano*, 2019, **13**, 2579–2586.
14 J. Huang, Z. Xu, W. Qiu, F. Chen, Z. Meng, C. Hou, W. Guo and X. Y. Liu, *Adv. Funct. Mater.*, 2020, **30**, 1910547.
15 A. M. Hussain, E. B. Lizardo, G. A. Torres Sevilla, J. M. Nassar and M. M. Hussain, *Adv. Healthcare Mater.*, 2015, **4**, 665–673.
16 A. H. Y. Lau, G. K. K. Chik, Z. Zhang, T. K. W. Leung and P. K. L. Chan, *Adv. Intell. Syst.*, 2020, **2**, 2000005.
17 N. S. Jang, K. H. Kim, S. H. Ha, S. H. Jung, H. M. Lee and J. M. Kim, *ACS Appl. Mater. Interfaces*, 2017, **9**, 19612–19621.
18 P. Won, J. J. Park, T. Lee, I. Ha, S. Han, M. Choi, J. Lee, S. Hong, K. J. Cho and S. H. Ko, *Nano Lett.*, 2019, **19**, 6087–6096.
19 R. Zhao, S. Lin, H. Yuk and X. Zhao, *Soft Matter*, 2018, **14**, 2515–2525.
20 S. K. Srivastava and Y. K. Mishra, *Nanomaterials*, 2018, **8**, 945.
21 R. Zhou, P. Li, Z. Fan, D. Du and J. Ouyang, *J. Mater. Chem. C*, 2017, **5**, 1544–1551.
22 B. W. An, E. J. Gwak, K. Kim, Y. C. Kim, J. Jang, J. Y. Kim and J. U. Park, *Nano Lett.*, 2016, **16**, 471–478.
23 R. Wang, Z. Xu, J. Zhuang, Z. Liu, L. Peng, Z. Li, Y. Liu, W. Gao and C. Gao, *Adv. Electron. Mater.*, 2017, **3**, 1600425.
24 Y. Chyan, R. Ye, Y. Li, S. P. Singh, C. J. Arnusch and J. M. Tour, *ACS Nano*, 2018, **12**, 2176–2183.
25 M. R. Bobinger, F. J. Romero, A. Salinas-Castillo, M. Becherer, P. Lugli, D. P. Morales, N. Rodríguez and A. Rivadeneyra, *Carbon*, 2019, **144**, 116–126.
26 J. Chen, Y. Wang, F. Liu and S. Luo, *ACS Appl. Mater. Interfaces*, 2020, **12**, 23284–23297.
27 A. Dallinger, K. Keller, H. Fitzek and F. Greco, *ACS Appl. Mater. Interfaces*, 2020, **12**, 19855–19865.
28 Y. Wang, Y. Wang, P. Zhang, F. Liu and S. Luo, *Small*, 2018, **14**, 1802350.
29 Y. Ling, W. Pang, X. Li, S. Goswami, Z. Xu, D. Stroman, Y. Liu, Q. Fei, Y. Xu, G. Zhao, B. Sun, J. Xie, G. Huang, Y. Zhang and Z. Yan, *Adv. Mater.*, 2020, **32**, 1908475.
30 Y. Wang, Z. Niu, J. Chen, Y. Zhai, Y. Xu and S. Luo, *Carbon*, 2019, **153**, 472–480.
31 W. Song, J. Zhu, B. Gan, S. Zhao, H. Wang, C. Li and J. Wang, *Small*, 2018, **14**, 1702249.
32 B. Ying, Q. Wu, J. Li and X. Liu, *Mater. Horiz.*, 2020, **7**, 477–488.
33 Z. Wang, K. Yu, G. Xie and J. Zou, *IOP Conf. Ser.: Earth Environ. Sci.*, 2018, **108**, 052094.
34 B. Ying, R. Z. Chen, R. Zuo, J. Li and X. Liu, *Adv. Funct. Mater.*, 2021, **31**, 2104665.
35 L. Tian, B. Zimmerman, A. Akhtar, K. J. Yu, M. Moore, J. Wu, R. J. Larsen, J. W. Lee, J. Li, Y. Liu, B. Metzger, S. Qu, X. Guo, K. E. Mathewson, J. A. Fan, J. Cornman, M. Fatina, Z. Xie, Y. Ma, J. Zhang, Y. Zhang, F. Dolcos, M. Fabiani, G. Gratton, T. Bretl, L. J. Hargrove, P. V. Braun, Y. Huang and J. A. Rogers, *Nat. Biomed. Eng.*, 2019, **3**, 194–205.
36 J. W. Lee, R. Xu, S. Lee, K.-I. Jang, Y. Yang, A. Banks, K. J. Yu, J. Kim, S. Xu, S. Ma, S. W. Jang, P. Won, Y. Li, B. H. Kim, J. Y. Choe, S. Huh, Y. H. Kwon, Y. Huang, U. Paik and J. A. Rogers, *Proc. Natl. Acad. Sci. U. S. A.*, 2016, **113**, 6131–6136.
37 X. Pu, M. Liu, X. Chen, J. Sun, C. Du, Y. Zhang, J. Zhai, W. Hu and Z. L. Wang, *Sci. Adv.*, 2017, **3**, 1700015.
38 L. M. Malard, M. A. Pimenta, G. Dresselhaus and M. S. Dresselhaus, *Phys. Rep.*, 2009, **473**, 51–87.
39 L. X. Duy, Z. Peng, Y. Li, J. Zhang, Y. Ji and J. M. Tour, *Carbon*, 2018, **126**, 472–479.
40 P. G. Agache, C. Monneur, J. L. Leveque and J. De Rigal, *Arch. Dermatol. Res.*, 1980, **269**, 221–232.
41 A. Rafsanjani, Y. Zhang, B. Liu, S. M. Rubinstein and K. Bertoldi, *Sci. Robot.*, 2018, **3**, eaar7555.
42 R. Sun, B. Zhang, L. Yang, W. Zhang, I. Farrow, F. Scarpa and J. Rossiter, *Appl. Phys. Lett.*, 2018, **112**, 251904.
43 S. Babaee, S. Pajovic, A. Rafsanjani, Y. Shi, K. Bertoldi and G. Traverso, *Nat. Biomed. Eng.*, 2020, **4**, 778–786.
44 H. Guo, M. H. Yeh, Y. C. Lai, Y. Zi, C. Wu, Z. Wen, C. Hu and Z. L. Wang, *ACS Nano*, 2016, **10**, 10580–10588.
45 S. Luo, P. T. Hoang and T. Liu, *Carbon*, 2016, **96**, 522–531.
46 R. W. Habash, R. Bansal, D. Krewski and H. T. Alhafid, *CRC Crit. Rev. Bioeng.*, 2006, **34**, 459–489.
47 M. E. E. Alahi, A. Nag, S. C. Mukhopadhyay and L. Burkitt, *Sens. Actuators, A*, 2018, **269**, 79–90.
48 W. Wang, L. Lu, Z. Li, L. Lin, Z. Liang, X. Lu and Y. Xie, *ACS Appl. Mater. Interfaces*, 2022, **14**, 1315–1325.
49 O. H. Yeoh, *Rubber Chem. Technol.*, 1993, **66**, 754–771.

